HHS Public Access

Author manuscript

J Comp Neurol. Author manuscript; available in PMC 2018 April 15.

Published in final edited form as:

J Comp Neurol. 2017 April 15; 525(6): 1403–1420. doi:10.1002/cne.23998.

Synaptic Organization of Striate Cortex Projections in the Tree Shrew: A Comparison of the Claustrum and Dorsal Thalamus

Jonathan D. Day-Brown[1], **Arkadiusz S. Slusarczyk**[2], **Na Zhou**[2], **Ranida Quiggins**[3], **Heywood M. Petry**[4], and **Martha E. Bickford**[2,*]

[1]Department of Psychology, Marshall University, Huntington WV [2]Department of Anatomical Sciences and Neurobiology, University of Louisville, Louisville, KY [3]Department of Anatomy, Chiang Mai University, Chiang Mai, Thailand [4]Department of Psychological and Brain Sciences, University of Louisville, Louisville, KY

Abstract

The tree shrew (*Tupaia belangeri*) striate cortex is reciprocally connected with the dorsal lateral geniculate nucleus (dLGN), the ventral pulvinar nucleus (Pv), and the claustrum. In the Pv and dLGN, striate cortex projections are thought to either strongly "drive", or more subtly "modulate" activity patterns respectively. To provide clues to the function of the claustrum, we compared the synaptic arrangements of striate cortex projections to the dLGN, Pv and claustrum using anterograde tracing and electron microscopy. Tissue was additionally stained with antibodies against gamma amino butyric acid (GABA) to identify GABAergic interneurons and nonGABAergic projection cells. The size of striate cortex terminals was largest in the Pv (0.94 ± 0.08 μm^2), intermediate in the claustrum (0.34 ± 0.02 μm^2) and smallest in the dLGN (0.24 ± 0.01 μm^2). Contacts on interneurons were most common in the Pv (39%), intermediate in the claustrum (15%) and least common in the dLGN (12%). In the claustrum, nonGABAergic terminals (0.34 ± 0.01 μm^2) and striate cortex terminals were not significantly different in size. The largest terminals in the claustrum were GABAergic (0.51 ± 0.02 μm^2) and these terminals contacted dendrites and somata that were significantly larger (1.90 ± 0.30 μm^2) than those contacted by cortex or nonGABAergic terminals (0.28 ± 0.02 μm^2 and 0.25 ± 0.02 μm^2 respectively). Our results indicate that the synaptic organization of the claustrum does not correspond with a driver/modulator framework. Instead, the circuitry of the claustrum suggests an integration of convergent cortical inputs, gated by GABAergic circuits.

Graphical abstract

*Correspondence: MDR Bldg Room 414A, 511 S. Floyd St., Louisville, KY 40202, martha.bickford@louisville.edu, 502-852-3527.

Conflict of interest statement: The authors have no known conflicts of interest that could inappropriately influence this work.

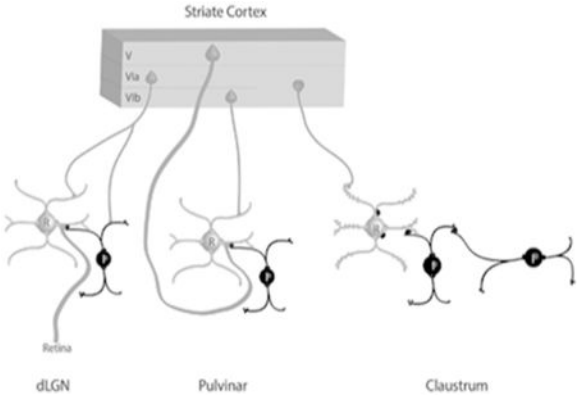

The schematic summary illustrates the contribution of terminals that originate from the tree shrew striate cortex to synaptic circuits in the dorsal lateral geniculate (dLGN), pulvinar nucleus and claustrum. Interneurons (I) and other elements that contain gamma amino butyric acid (GABA) are black. Thalamocortical and claustrocortical cells (relay cells, R), and other elements that are nonGABAergic, are gray. Circuits identified in the claustrum suggest an integration of convergent cortical inputs, gated by GABAergic circuits.

Keywords

pulvinar; dorsal lateral geniculate nucleus; corticoclaustral; GABA; synapse; retinogeniculate; corticothalamic; RRID:AB_94259; RRID:AB_258833; RRID:AB_477652; RRID: AB_2278725; RRID:AB_572256; RRID:AB_477329; RRID:AB_2333091; RRID: nif-000-30467

Introduction

The claustrum is an enigmatic structure of the telencephalon, interposed between the cerebral cortex and basal ganglia. Perhaps the most intriguing feature of the claustrum is that it is reciprocally connected with most areas of the cortex (for review see Goll, Atlan, & Citri, 2015). These vast connections have prompted speculation and study of the potential role of the claustrum in a variety of processes, including multisensory integration, attention allocation, novelty detection and consciousness (e.g. Edelstein and Denaro 2004; Crick and Koch 2005; Smythies et al. 2012; Remedios et al. 2014). However, there is relatively little information available regarding the specific functions of either claustrocortical or corticoclaustral connections.

The claustrum is a particularly well developed structure in the tree shrew (*Tupaia belangeri),* a species that is considered to represent a prototype of early prosimian primates. Although now classified in the order *Scadentia*, the brains of tree shrews display many primate-like features, particularly within visual structures (Holdefer and Norton 1995; Fitzpatrick 1996). In fact, reflecting the importance of vision for tree shrew behavior, cortical and subcortical visual structures make up a large proportion of the tree shrew brain. This elaboration of visual pathways is further demonstrated by the substantial reciprocal connections between the striate cortex and claustrum found in this species (Carey et al. 1979a, 1980; Carey and Neal 1986).

In addition to the claustrum, the striate cortex of the tree shrew is reciprocally connected with two other subcortical structures: the dorsal lateral geniculate nucleus (dLGN) and the ventral pulvinar nucleus (Pv, Carey et al. 1979b; Usrey et al. 1992; Usrey and Fitzpatrick 1996; Lyon et al. 2003). The striate cortex projections to these two thalamic nuclei arise from distinct cell types (Usrey and Fitzpatrick 1996), and it has been proposed that these corticothalamic projections carry out distinct functions. Because dLGN activity is primarily driven by direct input from the retina, corticogeniculate projections are considered to be "feedback" projections that do not dramatically alter receptive field properties, but instead modulate the responsiveness of dLGN neurons (Sherman and Guillery 1998; Briggs and Usrey 2008). In contrast, within the pulvinar nucleus, a population of corticopulvinar terminals has been found to be structurally and physiologically similar to retinogeniculate terminals (Guillery et al. 2001; Li, Guido, et al. 2003; Li, Wang, et al. 2003; Huppé-Gourgues et al. 2006). Therefore input from the striate cortex is thought to drive the receptive field properties of pulvinar neurons, and the striate-recipient zone of the pulvinar nucleus is recognized as a "higher order" thalamic nucleus to reflect this strong link to cortical rather than subcortical activity patterns (Sherman and Guillery 1998).

The purpose of this study was to directly compare the synaptic organization of projections from the striate cortex to the claustrum, dLGN and pulvinar nucleus of the same species in order to identify similarities or differences in these projections that may reveal clues to the function of the claustrum. In other words, we hoped to determine whether corticoclaustral projections display ultrastructural features that may be associated with "driving" (large terminals that innervate proximal dendrites) or "modulating" (smaller terminals that innervate more distal dendrites; inputs (reviewed in Bickford 2016). We additionally stained tissue sections to reveal the presence of gamma amino butyric acid (GABA). This allowed us to identify nonGABAergic projection cells and GABAergic interneurons within each structure, and determine the degree to which each of these cell types receive input from the striate cortex. Our results indicate that, although some similarities between claustrum and thalamic circuits can be identified, the synaptic organization of the claustrum does not suggest a driver/modulator framework. Instead, the circuitry of the claustrum suggests an integration of convergent cortical inputs, gated by GABAergic circuits.

Methods

A total of 11 adult tree shrews (*Tupaia belangeri*); 7 male and 4 female, (140 – 270 g) were used for these experiments. To label terminal projections from V1 by anterograde transport, 5 tree shrews received bilateral injections of biotinylated dextran amine (BDA; 3,000 MW, Molecular Probes, Eugene, OR) in the striate cortex. To label cells that project to V1 by retrograde transport, 4 shrews received bilateral injections of the beta subunit of cholera toxin (CTB; List Biological Laboratories, Inc. catalogue #105) in the striate cortex. Tissue from two additional animals was used for immunocytochemical staining of the claustrum. All methods were approved by the University of Louisville Animal Care and Use Committee and conform to the National Institutes of Health guidelines.

Tracer injections

Tree shrews that received neuroanatomical tracer injections were initially anesthetized with intramuscular injections of ketamine (100 mg/kg) and xylazine (6.7 mg/kg). Additional supplements of ketamine and xylazine were administered approximately every 45 minutes to maintain an appropriate depth of anesthesia through the completion of the injections. Prior to injection of the neuroanatomical tracer(s), the tree shrews were placed in a stereotaxic apparatus and prepared for sterile surgery. The heart rate was continuously monitored with a MouseOx pulse oximeter (STARR Life Sciences Corp., Pittsburgh, PA). A small area of the skull overlying V1 was removed and the dura reflected. Tracers were ejected using either iontophoretic or pressure injections. For iontophoretic injections (all BDA injections, and CTB injections in 2 animals), a glass pipette (tip diameter 2-10 μm) containing BDA (5% in saline), or CTB (1% desalted in 0.1M phosphate buffer (PB), pH 6.0) was lowered vertically and the tracer was ejected for 15-30 minutes using 2 μA continuous positive current. Pressure injections (CTB, 2% non-desalted, 0.3 μl) were made using a syringe pump equipped with a 5 μl microsyringe. The flow rate for the pressure injections was 150 nl per minute.

After a 7-day survival period, the tree shrews were given an overdose of ketamine (600 mg/kg) and xylazine (130 mg/kg) and perfused with Tyrode solution, followed by a fixative solution of 2% paraformaldehyde and 2% glutaraldehyde, or 4% paraformaldehyde in 0.1M PB (pH 7.4). The brain was removed from the skull, postfixed overnight in the perfusion fixative, sectioned to a thickness of 50 μm using a vibratome, and placed in 0.1 M phosphate buffer pH 7.4 (PB).

Histochemistry to reveal tracers

The BDA was revealed by incubating sections in a 1:100 dilution of avidin and biotinylated horseradish peroxidase (ABC; Vector Laboratories, Burlingame, CA) in phosphate-buffered saline (0.01 M PB with 0.9% NaCl, pH 7.4; PBS) overnight at 4° C. The sections were subsequently rinsed three times in PB (10 minutes each), reacted with nickel-intensified 3, 3′-diaminobenzidine (DAB) for 5 minutes, and washed in PB. The CTB was revealed using a rabbit-anti-CTB antibody (Table 1), followed by a biotinylated goat-anti-rabbit antibody (Vector, catalogue # BA-1000), ABC, and DAB reaction. DAB-labeled sections were either mounted on slides or prepared for electron microscopy as described below. A Neurolucida system and tracing software (MicroBrightField, Inc., Williston, VT) was used to plot the distribution of CTB-labeled thalamocortical and claustrocortical cells.

Electron microscopy

Sections that contained terminals labeled by the anterograde transport of BDA were postfixed in 2% osmium tetroxide, dehydrated in an ethyl alcohol series, and flat embedded in Durcupan resin between two sheets of Aclar plastic (Ladd Research, Williston, VT). Durcupan–embedded sections were first examined with a light microscope to select areas for electron microscopic analysis. Selected areas were mounted on blocks, ultrathin sections (70-80 nm, silver-gray interference color) were cut using a diamond knife, and sections were collected on Formvar-coated nickel slot grids. Selected sections were stained for the presence of gamma amino butyric acid (GABA). A postembedding immunocytochemical

protocol described previously (Chomsung et al. 2008, 2010; Day-Brown et al. 2010) was employed. Briefly, we used a rabbit polyclonal antibody against GABA (Table 1) that was tagged with a goat-anti-rabbit antibody conjugated to 15-nm gold particles (BBI Solutions USA, Madison, WI). The sections were air dried and stained with a 10% solution of uranyl acetate in methanol for 30 minutes before examination with an electron microscope.

Ultrastructural analysis

Ultrathin sections were examined using an electron microscope. Within each examined section, all labeled terminals involved in a synapse were imaged. The pre-and postsynaptic profiles were characterized on the basis of size (measured using Image J, RRID: nif-000-30467, or Maxim DL © 5 software), overlying gold particle density, and the presence or absence of synaptic vesicles. Since corticothalamic terminals are nonGABAergic (Li, Guido, et al. 2003; Jurgens et al. 2012) the gold particle density overlying BDA-labeled terminals was considered to be a measure of background staining. Profiles postsynaptic to BDA-labeled terminals were considered to be GABAergic if the overlying gold particle density was greater than the average density overlying all BDA-labeled profiles, and at least two times greater than the gold particle density overlying its presynaptic partner. For the analysis of non-BDA-labeled terminals and their postsynaptic profiles in the surrounding claustrum tissue, presynaptic and postsynaptic profiles were designated as GABAergic if their overlying gold density was at least two times greater than the average gold particle density overlying BDA-labeled terminals. Nonparametric two tailed Mann-Whitney tests were used for statistical analyses of ultrastructural data.

Immunohistochemistry for light microscopy

To reveal the borders of the claustrum, tissue sections were incubated overnight in a rat anti-substance P antibody, a mouse anti-calretinin antibody, a mouse anti-parvalbumin antibody, or a mouse anti-neuronal nitric oxide synthase antibody (Table 1). The next day the sections were incubated in biotinylated goat-anti-mouse, or biotinylated goat-anti-rat antibodies (1: 100, Vector) for 1 hour. The sections were subsequently incubated in ABC solution and reacted with DAB as describe above, and mounted on slides for light microscopic imaging.

To determine whether claustrocortical cells contain either glutamic acid decarboxylase (GAD) or parvalbumin, selected sections were incubated in a mouse-anti-GAD67 antibody or a mouse anti-parvalbumin antibody (Table 1) and the rabbit-anti-CTB simultaneously overnight. The next day the sections were incubated in a goat-anti-mouse antibody conjugated to Alexafluor-488 (1:100 Invitrogen, Waltham, MA) and a goat-anti-rabbit antibody conjugated to Alexafluor-546 (1:100 Invitrogen). Sections were then rinsed and mounted on slides and viewed using an Olympus confocal microscope.

Antibody characterization

The primary antibodies used in this study are listed in Table 1. The calretinin antibody recognized a single band of 31 kDa on immunoblot of ferret cochlear nucleus lysate (Fuentes-Santamaria et al. 2005). In the tree shrew claustrum, the calretinin antibody stains a small subset of cells, similar to previous descriptions in primates (Reynhout and Baizer 1999).

Using dot blot immunoassay, the CTB antibody was found to bind to cholera toxin, but showed no binding to Staphylococcus entrotoxin A, Staphylococcus entrotoxin B, or Pseudomonas exotoxin A (manufacturer's specification). In tree shrew tissue, staining with the CTB antibody was located only within the striate cortex injection sites and in brain regions that project to the striate cortex.

The GABA antibody shows positive binding with GABA and GABA-keyhole limpet hemocyanin, but not bovine serum albumin (BSA), in dot blot assays (manufacturer's product information). In tree shrew tissue, the GABA antibody stains a subset of neurons in the dorsal thalamus and cortex (Chomsung et al. 2008, 2010). This labeling pattern is consistent with other GABAergic markers used in a variety of species (Bickford et al. 1999).

The GAD antibody recognizes a single band at 67kDa on Western blot analysis of rat brain (manufacturer's communication). In cat and tree shrew tissue, this antibody stains most neurons in the thalamic reticular nucleus and a subset of neurons in the dorsal thalamus (Bickford et al. 2008; Chomsung et al. 2008).

Western blot analysis of brain homogenates shows the neuronal nitric oxide synthase antibody specifically labels a band of approximately 155kDa, and immunolabeling is abolished by preadsorption with synthetic human nitric oxide synthase at 5 μg/ml of diluted antibody (manufacturer's information). The neuronal nitric oxide synthase antibody stains a subset of neurons in the pedunculopontine tegmentum in mouse (Kohlmeier et al. 2012) and tree shrew.

The parvalbumin antibody recognizes a single band of ~12 kDa on western blot analysis of extracts from fish skeletal muscle (data provided by Sigma-Aldrich). The specificity of this antibody for the antigen has been determined by preadsorption with the appropriate purified protein as described by others (Hackney et al. 2005). In the tree shrew claustrum, the parvalbumin antibody stains a subset of cells, similar to previous descriptions in primates (Reynhout and Baizer 1999).

Using radioimmunoassays, the substance P antibody was found to specifically bind substance P, and other neuropeptides (leu-enkephalin, met-enkephalin, somatostatin and ß-endorphin) did not compete with this binding (Cuello et al. 1979). The substance P antibody stains tectothalamic terminals in the rat lateral posterior nucleus and electrical stimulation of these terminals activates neurokinin receptors (Masterson et al. 2010).

Results

Location and cytoarchitecture of the tree shrew dorsal claustrum

Figure 1 illustrates the location of the tree shrew dorsal claustrum (Cld, defined by Carey et al. 1979, 1980; Carey and Neal 1986) in sections stained with antibodies against calretinin (A-D and J), substance P (E-H and I), neuronal nitric oxide synthase (K) and parvalbumin (L). As previously described for the cat claustrum (Rahman and Baizer 2007; Hinova-Palova et al. 2008), antibodies against calretinin, neuronal nitric oxide synthase, and parvalbumin stain subpopulations of nonspiny cells within the claustrum (Figure 1J-L), while the

substance P antibody stained axon terminals (Figure 1I). We found that staining with the substance P antibody most clearly delineated the Cld from the surrounding cortex, caudate and putamen (Figure 1E-H). Adjacent sections stained with the calretinin antibody reveal the Cld as a region more lightly stained than the underlying cortex surrounding the rhinal sulcus (Figure 1A-D).

Thalamocortical and claustrocortical cells that project to V1

Following injections of CTB in V1 (Figure 2A), cells labeled by retrograde transport were distributed in the Cld (Figure 2C-H and 3B), dLGN and Pv (Figures 2I-L and 3A). Of these nuclei, the Cld contained the largest population of retrogradely labeled cells. Following bilateral CTB injections in V1 of one tree shrew, we plotted all subcortical labeled cells in 70 μm thick sections that were spaced 350 μm apart. In this series, the Cld contained 2753 labeled cells, the Pv contained 905 labeled cells, and the dLGN contained 215 labeled cells. Thus, as illustrated by the Figure 2B histogram, the numbers of Cld cells that project to a given site within V1 far outweigh the number of thalamocortical cells that project to the same site.

To determine whether Cld-V1 cells are GABAergic, we stained sections containing CTB-labeled Cld-V1 cells with an antibody against glutamic acid decarboxylase (GAD). As illustrated in Figure 3 (E, F), no CTB-labeled Cld-V1 cells were found to contain GAD (0 of 675 CTB-labeled cells examined). We also stained sections that contained CTB-labeled cells with an antibody against parvalbumin (Figure 3 C,D) and found that no Cld-V1 cells stained for parvalbumin (0 of 583 CTB-labeled cells examined). Therefore, like thalamocortical projection cells (Montero 1986), the Cld-V1 projection is nonGABAergic. This also suggests that within the Cld, GABAergic cells, and cells that contain parvalbumin, are likely to be interneurons.

Morphology of striate cortex projections to the dorsal thalamus and claustrum

Injections of BDA in V1 (Figure 2A) labeled terminals in the claustrum and dorsal thalamus that display distinct morphologies. Corticothalamic terminals in the dLGN (Figure 4A) form small boutons that emanate from relatively thin axons (class I, Guillery 1966). Corticothalamic terminals in Pv (Figure 4B) primarily emanate from thicker axons to form sparsely distributed “grape-like” clusters of larger terminals (class II, Guillery 1966). Corticoclaustral axons formed either very small boutons distributed along axons in a “beads-on-a-string” manner (arrowheads, Figure 4C), or slightly larger terminals that formed dense clusters (arrow, Figure 4C).

Ultrastructure of striate cortex projections to the dLGN

A total of 207 corticogeniculate terminals that were involved in synapses (case 5, n =102, case 6, n = 105) were examined as described in the Methods. The terminals were small and contained densely packed round vesicles (Figure 5A, B). Thus, these terminals can be described as RS profiles (a term previously used to describe the ultrastructure of class I terminals; Guillery 1969). The average size of corticogeniculate terminals (Figure 6A) was $0.24 \pm 0.01\ \mu m^2$, and the average size of profiles postsynaptic to corticogeniculate terminals (Figure 6B) was $0.73 \pm 0.05\ \mu m^2$. The overwhelming majority of corticogeniculate terminals

were found to make relatively simple, one to one connections (96.6%, the remaining synapses were classified as perforated). No postsynaptic profiles were found to contain vesicles. Analysis of gold particle density (as described in the methods) revealed that the majority (88.4%) of postsynaptic profiles were nonGABAergic (Figure 6C).

Ultrastructure of striate cortex projections to the Pv

A total of 101 corticopulvinar profiles involved in synapses (case 5 n=42, case 6 n=59) were examined. These 101 presynaptic terminals contacted 131 postsynaptic profiles. Thus, 27.7% of corticopulvinar terminals contacted multiple postsynaptic profiles. Additionally, 11.9% of presynaptic profiles were found to make perforated synapses. Therefore, 60.4% of corticopulvinar terminals were found to be simple one-to-one contacts.

Corticopulvinar terminals were significantly larger than corticogeniculate terminals (average size of corticopulvinar terminals = 0.94 ± 0.08 μm^2, p<.0001; Figure 6A). These large terminals contained densely packed round vesicles (Figure 5C-F) and can therefore be described as RL profiles (a term previously applied to describe the ultrastructure of type II terminals; Guillery et al. 2001). Corticopulvinar terminals contacted GABAergic profiles more frequently (38.9%; Figure 6C) than did corticogeniculate terminals (11.6%), and the majority of these GABAergic postsynaptic profiles contained vesicles (84.8%; Figure 5E,F). These profiles are therefore classified as F2 profiles (Guillery 1969). The sizes of profiles postsynaptic to corticopulvinar terminals were not significantly different (p = 0.7296) from that of profiles postsynaptic to corticogeniculate terminals (average size of corticopulvinar postsynaptic profiles = 0.75 ± 0.06 μm^2).

Ultrastructure of striate cortex projections to the claustrum

A total of 189 corticoclaustral terminals involved in synapses were examined (case 5 n=132, case 6 n=57). The majority (98.9%) of presynaptic terminals contacted a single postsynaptic profile. Corticoclaustral terminals were significantly larger (mean = 0.34 ± 0.02 μm^2) than corticogeniculate terminals (p<0.0001, Figure 6A). These terminals typically contacted small caliber dendrites and spines that were significantly smaller than the dendrites contacted by terminals in either the dLGN or Pv (mean = 0.28 ± 0.02 μm^2, both p<0.0001; Figure 6B). While the majority (88.2%) of synaptic contacts were simple one-to-one connections, a small proportion (11.8%) formed perforated synaptic contacts. Corticoclaustral terminals primarily contacted nonGABAergic postsynaptic profiles (Figure 7A-H); however, 15.2% of the terminals contacted GABAergic profiles (Figure 7I-K; Figure 6C).

General ultrastructure of the claustrum

To compare terminals that originate from the striate cortex to the general population of GABAergic and nonGABAergic terminals within the claustrum, we measured GABAergic and nonGABAergic terminals and their postsynaptic targets in the tissue surrounding the BDA-labeled corticoclaustral terminals (n = 119 GABAergic and 244 nonGABAergic terminals). Figure 8 illustrates the ultrastructure of nonGABAergic profiles in the claustrum. NonGABAergic presynaptic profiles (Figure 8, A-F, yellow) contained either sparse (Figure

8A, B) or densely-packed vesicles (Figure 8C-F) and primarily contacted relatively small caliber dendrites (Figure 8, A-F, green).

Some GABAergic terminals could be identified as originating from dendrites (Figure 9 A-D, purple). These dendrites contained vesicles clustered at presynaptic sites (Figure 9 B,D). GABAergic dendritic terminals contacted nonGABAergic dendrites (A, B, green) and GABAergic dendrites (B, D, blue). Other GABAergic terminals (Figure 9 E-G, red), which presumably arise from axons, primarily contact nonGABAergic dendrites (E-F, green) and somata (G, green).

The size of corticoclaustral terminals was not significantly different from the size of the general population of nonGABAergic terminals in the claustrum (mean = 0.34 ± 0.01 μm^2, p = 0.2111, Figure 6D), although the size of dendrites postsynaptic targets to nonGABAergic terminals was slightly smaller than those postsynaptic to cortical terminals (0.25 ± 0.02 μm^2, p = 0.0174; Figure 6E). In contrast, GABAergic terminals (0.51 ± 0.02 μm^2) were much larger than both nonGABAergic terminals ($p < 0.0001$; Figure 6D) or corticoclaustral terminals ($p < 0.0001$ Figure 6D). Likewise, the postsynaptic targets of GABAergic terminals were much larger (1.90 ± 0.30 μm^2; Figure 6E) than those of nonGABAergic terminals ($p < 0.0001$) or corticoclaustral terminals ($p < 0.0001$). Finally, 9.8% of nonGABAergic terminals contacted GABAergic profiles and 9.2% of GABAergic terminals contacted GABAergic profiles (Figure 6F).

Discussion

Summary

We compared inputs from the striate cortex to the Pv, dLGN and Cld (schematically summarized in Figure 10). Our results indicate that corticoclaustral terminals are much smaller than corticopulvinar “driving” inputs, and slightly larger than corticogeniculate “modulating” inputs. When we examined the overall population of terminals in the claustrum, we found that the size and synaptic targets of corticoclaustral terminals were not significantly different from the total population of nonGABAergic terminals. Therefore, the circuitry of the claustrum does not support the concept of a single prominent glutamatergic input that determines receptive field properties. Instead, we found that the largest inputs to the claustrum are GABAergic terminals. Furthermore, within the claustrum GABAergic terminals frequently synapse on somata and proximal dendrites, whereas nonGABAergic terminals primarily target small dendrites and spines. Thus, the synaptic organization of the claustrum suggests an integration of cortical inputs, possibly gated by GABAergic circuits.

Comparison with previous studies of visual cortex connections with the dorsal thalamus

The results of our retrograde tracing experiments were similar to previous experiments carried out in the tree shrew. Injections of retrograde tracers in the striate cortex labeled cells in restricted regions of the dLGN, ventral regions of the pulvinar nucleus, and in a strip of cells termed the lateral intermediate nucleus (Diamond et al. 1970; Carey et al. 1979b). In his extensive study of thalamic projections to visual areas of the tree shrew cortex, Lyon et

al. (2003) described a similar pattern, but included the lateral intermediate nucleus as part of the Pv, and we have adopted this nomenclature in the current study.

The ultrastructural features of striate cortex projections to the tree shrew dLGN and Pv were similar to those examined in previous electron microscopic studies of the dLGN and striate recipient regions of the pulvinar (or lateral posterior, LP) nucleus of rodents (Li, Wang, et al. 2003; Bickford et al. 2015), carnivores (Vidnyánszky and Hámori 1994; Vidnyánszky et al. 1996; Erişir et al. 1997; Feig and Harting 1998; Guillery et al. 2001; Huppé-Gourgues et al. 2006), and primates (Ogren and Hendrickson 1979; Feig and Harting 1998). In each of these species, corticogeniculate projections from V1 form small terminals, the majority of which contact nonGABAergic dendrites, while corticopulvinar terminals form large terminals that contact both relay cell dendrites and the GABAergic dendritic terminals of interneurons (F2 profiles) in complex synaptic arrangements (glomeruli).

In rodents, *in vitro* studies have established that corticogeniculate and cortico-LP terminals display very different synaptic properties (Granseth et al. 2002; Li, Guido, et al. 2003; Jurgens et al. 2012). When corticogeniculate (type I) axons are stimulated with increasing current levels, the resulting excitatory postsynaptic potentials (EPSPs) increase in amplitude in a graded manner, demonstrating that multiple corticogeniculate axons converge to innervate each cell. In contrast, when type II cortico-LP axons are stimulated with increasing current levels, the EPSP amplitudes increase in an “all-or-none” manner, indicating that each cell is innervated by only a few type II axons. In addition, repetitive stimulation of type I axons increases EPSP amplitudes in a frequency-dependent manner, while repetitive stimulation of type II axons decreases EPSP amplitudes. Since the ultrastructure of cortico-LP terminals and synaptic responses elicited by their stimulation are similar to those of retinogeniculate terminals (Chen et al. 2002; Li, Wang, et al. 2003), it has been proposed that the pulvinar nucleus is driven by cortical input, and perhaps functions to transfer information from one cortical area to another (Sherman and Guillery 1998). However, the exact role of corticopulvinar terminals remains somewhat of an open question; recent analyses of receptive field properties in the striate-recipient zone of the cat LP nucleus suggest that, rather than mimicking the properties of V1 cells that project to this region, the receptive field properties of LP neurons likely result from a high degree of integration of cortical inputs (Piché et al. 2015).

Comparison with previous studies of visual cortex connections with the claustrum

The distribution of cells labeled in the tree shrew claustrum via the retrograde transport of CTB injected into the striate cortex was very similar to that observed by Carey et al. (1979b, 1980) following injections of the horseradish peroxidase in the striate cortex. They found that claustrum cells that project to the striate cortex were distributed in the most dorsal parts of the tree shrew claustrum, which they termed the Cld, and we have adopted this nomenclature in the current study. In the cat, projections to visual areas of the cortex also originate from the dorsal parts of the claustrum (LeVay and Sherk 1981; Sherk and LeVay 1981; Olson and Graybiel 1983).

The cells in the claustrum can be divided into spiny projection neurons and nonspiny interneurons (LeVay and Sherk 1981; Wasilewska and Najdzion 2001). We found that

claustral cells that project to the striate cortex did not contain GAD, which suggests that GABAergic cells within the claustrum are interneurons. In support of this, we found that presynaptic dendrites in the claustrum contain GABA. A variety of calcium binding proteins, neuropeptides and enzymes are found within the nonspiny neurons of the claustrum (Druga et al.1993; Hinova-Palova et al. 1997, 2007, 2008, 2012; Reynhout and Baizer 1999; Rahman and Baizer 2007; Baizer et al. 2014; Kim et al., 2016). We also found that cells in the tree shrew claustrum stained with antibodies against parvalbumin, neuronal nitric oxide synthase or calretinin did not exhibit spines. Future studies are needed to determine whether GABA is contained within this wide variety of potential interneuron cell types, or restricted to specific interneuron populations.

Previous electron microscopy studies in the cat examined corticoclaustral terminals using degeneration techniques (Juraniec et al. 1971; LeVay and Sherk 1981; Kubasik-Juraniec et al. 1994). These studies found that corticoclaustral terminals primarily contact small dendrites and spines, similar to our results in the tree shew. LeVay and Sherk (1981) also identified some degenerating terminals that contacted beaded dendrites, which could have arisen from interneurons. By combining anterograde tracing and immuoncytochemical localization of GABA, we found that 15% of corticoclaustral terminals contacted GABAergic dendrites. This is most likely an underestimate of the percentage of corticoclaustral terminals that contact GABAergic profiles; our conservative method of analysis may have incorrectly designated very small postsynaptic profiles as nonGABAergic. A serial section analysis would be necessary to more accurately establish the full extent of cortical input to GABAergic neurons in the claustrum. Recently, Kim et al (2016) found that within the mouse claustrum, 73% of claustrocortical cells and 73% of parvalbumin interneurons responded to optogenetic activation of corticoclaustral terminals.

LeVay and Sherk (1981) also compared corticoclaustral terminals to the overall population of boutons that display a prominent postsynaptic density (Gray's type I) and found no differences in the synaptic contacts of these boutons when compared to degenerating corticoclaustral terminals. Similarly, when we compared BDA-labeled corticoclaustral terminals to the overall population of nonGABAergic terminals in the tree shrew claustrum, we found no differences in the size of these terminals or their postsynaptic targets. We also found that nonGABAergic terminals and corticoclaustral terminals contacted similar numbers of GABAergic and nonGABAergic profiles. Thus, to date, all evidence indicates that small nonGABAergic terminals, which include those that originate from the cortex, primarily innervate the smaller (presumably more distal) dendrites and spines of claustrocortical cells.

Other sources of nonGABAergic inputs in the claustrum may include the axon collaterals of claustrocortical cells, the thalamus, amygdala, or dorsal raphe nucleus (LeVay and Sherk 1981; Carey and Neal 1986; Goll et al. 2015; Kim et al., 2016). While we found that the majority of nonGABAergic terminals displayed features similar to corticoclaustral terminals, we did find that the density of vesicles was much lower in some nonGABAergic terminals (Figure 8A, B). This feature was previously noted by Norita and Hirata (1976) in the cat claustrum (their type B terminal). Additional studies will be necessary to determine whether this ultrastructure feature correlates with a specific input source. Nonetheless, the sparse-

vesicle nonGABAergic terminal type, like corticoclaustral terminals, primarily contacts small dendrites and spines. Therefore, our studies, and those conducted previously in the cat, show no evidence of any nonGABAergic terminals similar to the “driver” inputs identified in the dorsal thalamus.

GABAergic circuits within the claustrum—Our study is the first to examine GABAergic circuits within the claustrum using electron microscopy. In comparison to nonGABAergic terminals, we found that the overall population of GABAergic terminals was larger and more frequently contacted larger (presumably more proximal) nonGABAergic dendrites and somata. Thus, within the claustrum, GABAergic terminals are ideally positioned to shunt, or gate, the postsynaptic responses generated by cortical inputs to the more distal dendritic arbors of claustrocortical cells. Similar arrangements of GABAergic terminals have been shown to significantly affect the firing properties of their postsynaptic partners. For example, in the caudate and putamen, inputs from the cortex and thalamus are highly convergent and primarily target the spines of medium spiny neurons, while GABAergic inputs are much less numerous and target more proximal dendrites and somata (Wilson 2007). In this case, even though GABAergic inputs contribute a small fraction of the input to each spiny neuron, they can have a very potent impact on their firing properties. Likewise, in the cortex, glutamatergic synaptic inputs onto the spines of pyramidal cells far outweigh GABAergic inputs, but because GABAergic synapses are more concentrated on somata and axon initial segments, they can strongly suppress pyramidal cell activity (Harris and Shepard 2015). Finally, we found evidence for GABAergic dendritic terminals as well as evidence of connections between GABAergic dendrites. This indicates that GABAergic interneurons within the claustrum could form an interconnected network that could regulate activity patterns through a complex mix of inhibition and disinhibition. A recent optogenetic study confirms that claustrocortical cells and GABAergic parvalbumin interneurons are highly interconnected within the mouse claustrum (Kim et al., 2016).

Claustrum and thalamic connections with the cortex

As discussed previously (Olson and Graybiel 1980; Goll et al. 2015), the claustrum is similar to the dorsal thalamus in that it is reciprocally connected with the cerebral cortex, and projections to and from different sensory regions of the cortex are segregated in both the dorsal thalamus and the claustrum. Our study indicates that there is a significant difference in the number of cells labeled in each of these regions by retrograde transport from single injections in the striate cortex. Unfortunately, we cannot comment on ipsilateral versus contralateral projection patterns because bilateral tracer injections were placed in V1 of all animals used for this study. Previous studies have shown that the claustrocortical projection is primarily ipsilateral, but injections of retrograde tracers in V1 also label cells in the contralateral claustrum (LeVay and Sherk 1981). If ipsilateral and contralateral projections arise from different cells in the claustrum, our bilateral injections would have contributed to the large number of cells labeled in the claustrum relative to the thalamus (which projects only to the ipsilateral cortex).

Nonetheless, our retrograde tracing results suggest differences in the topography of projections from the dLGN, Pv and claustrum. Cells in the dLGN project to very restricted

regions of the striate cortex (Raczkowski and Fitzpatrick 1990); potentially individual Pv and claustrum cells innervate larger regions of the cortex. We previously examined the projections from the dorsal (Pd) and central (Pc) regions of the tree shrew pulvinar and found that small injections in each subdivision labeled terminal projections in two separate regions of the temporal cortex, as well as the striatum and amygdala (Chomsung et al. 2010; Day-Brown et al. 2010). Rockland et al. (1999) also found that single pulvinar axons in the primate innervate multiple visual cortical areas. Pv cells are labeled following injections in V1, V2, and temporal areas of the visual cortex (Carey et al. 1979b; Lyon et al. 2003) as well as the claustrum (Carey and Neal 1986). Individual claustrocortical axons are very fine, form very sparse boutons, and limited reconstructions suggest that they diffusely innervate V1 (LeVay 1986; da Costa et al. 2010). Double labeling studies in mice suggest that the axons of individual claustrocortical neurons can branch to innervate both sensory and motor cortical areas (Smith et al. 2012).

A number of previous studies have found that corticoclaustral, corticogeniculate and corticopulvinar projections originate from separate cell groups. Corticogeniculate cells are pyramidal cells located primarily in layer VIa, while corticopulvinar cells are pyramidal cells located in layers VIb and V (Conley and Raczkowski 1990; Usrey and Fitzpatrick 1996). Corticoclaustral cells are located in layer VI and display an “inverted” morphology (Carey et al. 1980; Katz 1987; Bueno-López et al. 1991). Our results contribute to the characterization of these distinct cell types by demonstrating that their axon projections form terminals of different sizes that each participate in unique synaptic circuits (Figure 10).

Claustral circuits and theories of claustrum function—Because the claustrum is reciprocally connected to most cortical areas, it has been suggested that multimodal integration within this structure may bind features to form a seamless percept (Smythies et al. 2012). This idea was elaborated by Crick and Koch (2005) to advocate a key role for the claustrum in the state of consciousness. However, while the claustrum as a whole exhibits multimodal responses (Smythies et al., 2014), connections with the visual, auditory and somatosensory cortices are segregated within the claustrum (Olson and Graybiel 1980). Furthermore, recordings from single neurons within the claustrum have not revealed any multimodal responses. Instead, cells in the claustrum exhibit low rates of spontaneous activity and respond transiently, in a modality-specific manner, to the appearance of novel stimuli (Remedios et al. 2010, 2014). In the visual sector of the claustrum, the movement of stimuli is necessary to elicit maximal responses (Sherk and LeVay 1981). These results have led to the more recent proposition that the claustrum functions as a novelty detector, to facilitate rapid shifts in attention (Remedios et al. 2014; Goll et al. 2015).

The claustrum circuits that we identified fit well with this concept. The intrinsic GABAergic network could maintain low spontaneous activity, which is overcome only briefly when a novel sensory stimulus appears. Although the brief bursts of activity in the claustrum are modality specific, branching projections of claustrum cells to sensory and related motor areas of the cortex could function to facilitate the coordination of sensory perception and motor reactions (Smith et al. 2012). In the tree shrew, the coordination of vision and action is particularly important, to assure that this fast moving species accurately navigates its

environment to catch insects and avoid predators. If, in fact, the claustrum is involved in such coordination, this may explain why this structure is so prominent in tree shrews.

Acknowledgments

The authors thank Phillip S. Maire and the University of Louisville veterinary staff for maintenance of the tree shrew colony and assistance with surgical procedures.

Role of authors: All authors had full access to all the data in the study and take responsibility for the integrity of the data and the accuracy of the data analysis. Study concept and design: JDD-B, HMP, MEB. Acquisition of data: JDD-B, ASS, NZ, RQ, MEB. Analysis and interpretation of data: JDD-B, ASS, NZ, MEB. Critical revision of the manuscript for important intellectual content: JDD-B, HMP, MEB. Statistical analysis: JDD-B, NZ Obtained funding: MEB, HMP. Administrative, technical, and material support: MEB, ASS. Study supervision: MEB.

Funding: This work was supported by the National Institutes of Health, grant numbers R01EY016155 and R21EY021016

References cited

Baizer JS, Sherwood CC, Noonan M, Hof PR. Comparative organization of the claustrum: what does structure tell us about function? Front Syst Neurosci. 2014; 8:117. [PubMed: 25071474]

Bickford ME, Carden WB, Patel NC. Two types of interneurons in the cat visual thalamus are distinguished by morphology, synaptic connections, and nitric oxide synthase content. J Comp Neurol. 1999; 413:83–100. [PubMed: 10464372]

Bickford ME, Wei H, Eisenback Ma, Chomsung RD, Slusarczyk AS, Dankowski AB. Synaptic organization of thalamocortical axon collaterals in the perigeniculate nucleus and dorsal lateral geniculate nucleus. J Comp Neurol. 2008; 508:264–285. [PubMed: 18314907]

Bickford ME, Zhou N, Krahe TE, Govindaiah G, Guido W. Retinal and Tectal "Driver-Like" Inputs Converge in the Shell of the Mouse Dorsal Lateral Geniculate Nucleus. J Neurosci. 2015; 35:10523–10534. [PubMed: 26203147]

Bickford ME. Thalamic circuit diversity: modulation of the driver/modulator framework. Frontiers in Neural Circuits. 2016; 9:86.doi: 10.3389/fncir.2015.00086 [PubMed: 26793068]

Briggs F, Usrey WM. Emerging views of corticothalamic function. Curr Opin Neurobiol. 2008; 18:403–407. [PubMed: 18805486]

Bueno-López JL, Reblet C, López-Medina A, Gómez-Urquijo SM, Grandes P, Gondra J, Hennequet L. Targets and Laminar Distribution of Projection Neurons with "Inverted" Morphology in Rabbit Cortex. Eur J Neurosci. 1991; 3:415–430. [PubMed: 12106181]

Carey RG, Bear MF, Diamond IT. The laminar organization of the reciprocal projections between the claustrum and striate cortex in the tree shrew, Tupaia glis. Brain Res. 1980; 184:193–198. [PubMed: 7357417]

Carey RG, Fitzpatrick D, Diamond IT. Layer I of striate cortex of Tupaia glis and Galago senegalensis: projections from thalamus and claustrum revealed by retrograde transport of horseradish peroxidase. J Comp Neurol. 1979a; 186:393–437. [PubMed: 110851]

Carey RG, Fitzpatrick D, Diamond IT. Layer I of striate cortex of Tupaia glis and Galago senegalensis: projections from thalamus and claustrum revealed by retrograde transport of horseradish peroxidase. J Comp Neurol. 1979b; 186:393–437. [PubMed: 110851]

Carey RG, Neal TL. Reciprocal connections between the claustrum and visual thalamus in the tree shrew (Tupaia glis). Brain Res. 1986; 386:155–168. [PubMed: 3779407]

Chen C, Blitz DM, Regehr WG. Contributions of receptor desensitization and saturation to plasticity at the retinogeniculate synapse. Neuron. 2002; 33:779–788. [PubMed: 11879654]

Chomsung RD, Petry HM, Bickford ME. Ultrastructural examination of diffuse and specific tectopulvinar projections in the tree shrew. J Comp Neurol. 2008; 510:24–46. [PubMed: 18615501]

Chomsung RD, Wei H, Day-Brown JD, Petry HM, Bickford ME. Synaptic organization of connections between the temporal cortex and pulvinar nucleus of the tree shrew. Cereb Cortex. 2010; 20:997–1011. [PubMed: 19684245]

Conley M, Raczkowski D. Sublaminar organization within layer VI of the striate cortex in Galago. J Comp Neurol. 1990; 302:425–436. [PubMed: 1705271]

Crick FC, Koch C. What is the function of the claustrum? Philos Trans R Soc Lond B Biol Sci. 2005; 360:1271–1279. [PubMed: 16147522]

Cuello AC, Galfre G, Milstein C. Detection of substance P in the central nervous system by a monoclonal antibody. Proc Natl Acad Sci U S A. 1979; 76:3532–3536. [PubMed: 386341]

da Costa NM, Fürsinger D, Martin KaC. The synaptic organization of the claustral projection to the cat's visual cortex. J Neurosci. 2010; 30:13166–13170. [PubMed: 20881135]

Day-Brown JD, Wei H, Chomsung RD, Petry HM, Bickford ME. Pulvinar projections to the striatum and amygdala in the tree shrew. Front Neuroanat. 2010; 4:143. [PubMed: 21120139]

Diamond IT, Snyder M, Killackey H, Jane J, Hall WC. Thalamo-cortical projections in the tree shrew (Tupaia glis). J Comp Neurol. 1970; 139:273–306. [PubMed: 5433195]

Druga R, Chen S, Bentivoglio M. Parvalbumin and calbindin in the rat claustrum: an immunocytochemical study combined with retrograde tracing frontoparietal cortex. J Chem Neuroanat. 1993; 6:399–406. [PubMed: 8142075]

Edelstein LR, Denaro FJ. The claustrum: a historical review of its anatomy, physiology, cytochemistry and functional significance. Cell Mol Biol (Noisy-legrand). 2004; 50:675–702.

Erişir, a, Van Horn, SC., Sherman, SM. Relative numbers of cortical and brainstem inputs to the lateral geniculate nucleus. Proc Natl Acad Sci U S A. 1997; 94:1517–1520. [PubMed: 9037085]

Feig S, Harting JK. the Thalamus : Ultrastructural Studies of Corticothalamic Projections From Area 17 to the Lateral Posterior Nucleus of the Cat and Inferior Pulvinar. 1998; 295:281–295.

Fitzpatrick D. The functional organization of local circuits in visual cortex: insights from the study of tree shrew striate cortex. Cereb Cortex. 1996; 6:329–341. [PubMed: 8670661]

Fuentes-Santamaria V, Alvarado JC, Taylor AR, Brunso-Bechtold JK, Henkel CK. Quantitative changes in calretinin immunostaining in the cochlear nuclei after unilateral cochlear removal in young ferrets. J Comp Neurol. 2005; 483:458–475. [PubMed: 15700274]

Goll Y, Atlan G, Citri A. Attention: the claustrum. Trends Neurosci. 2015; 38:486–495. [PubMed: 26116988]

Granseth B, Ahlstrand E, Lindström S. Paired pulse facilitation of corticogeniculate EPSCs in the dorsal lateral geniculate nucleus of the rat investigated in vitro. J Physiol. 2002; 544:477–486. [PubMed: 12381820]

Guillery RW. A study of Golgi preparations from the dorsal lateral geniculate nucleus of the adult cat. J Comp Neurol. 1966; 128:21–49. [PubMed: 4165857]

Guillery RW. The organization of synaptic interconnections in the laminae of the dorsal lateral geniculate nucleus of the cat. Z Zellforsch Mikrosk Anat. 1969; 96:1–38. [PubMed: 5772028]

Guillery RW, Feig SL, Van Lieshout DP. Connections of higher order visual relays in the thalamus: a study of corticothalamic pathways in cats. J Comp Neurol. 2001; 438:66–85. [PubMed: 11503153]

Hackney CM, Mahendrasingam S, Penn A, Fettiplace R. The concentrations of calcium buffering proteins in mammalian cochlear hair cells. J Neurosci. 2005; 25:7867–7875. [PubMed: 16120789]

Harris KD, Shepherd GM. The neocortical circuit: themes and variations. Nat Neurosci. 2015; 18(20): 170–81. [PubMed: 25622573]

Hinova-Palova D, Edelstein L, Paloff A, Hristov S, Papantchev V, Ovtscharoff W. Neuronal nitric oxide synthase immunopositive neurons in cat claustrum--a light and electron microscopic study. J Mol Histol. 2008; 39:447–457. [PubMed: 18685959]

Hinova-Palova D, Edelstein L, Papantchev V, Landzhov B, Malinova L, Todorova-Papantcheva D, Minkov M, Paloff A, Ovtscharoff W. Light and electron-microscopic study of leucine enkephalin immunoreactivity in the cat claustrum. J Mol Histol. 2012; 43:641–649. [PubMed: 22972434]

Hinova-Palova DV, Edelstein LR, Paloff AM, Hristov S, Papantchev VG, Ovtscharoff WA. Parvalbumin in the cat claustrum: ultrastructure, distribution and functional implications. Acta Histochem. 2007; 109:61–77. [PubMed: 17126385]

Hinova-Palova DV, Paloff A, Christova T, Ovtscharoff W. Topographical distribution of NADPH-diaphorase-positive neurons in the cat's claustrum. Eur J Morphol. 1997; 35:105–116. [PubMed: 9253588]

Holdefer RN, Norton TT. Laminar organization of receptive field properties in the dorsal lateral geniculate nucleus of the tree shrew (Tupaiaglis belangeri). J Comp Neurol. 1995; 358:401–413. [PubMed: 7560294]

Huppé-Gourgues F, Bickford ME, Boire D, Ptito M, Casanova C. Distribution, morphology, and synaptic targets of corticothalamic terminals in the cat lateral posterior-pulvinar complex that originate from the posteromedial lateral suprasylvian cortex. J Comp Neurol. 2006; 497:847–863. [PubMed: 16802329]

Juraniec J, Narkiewica O, Wrzolkowa T. Axon terminals in the claustrum of the cat: an electron microscope study. Brain Res. 1971; 35:277–282. [PubMed: 5134234]

Jurgens CWD, Bell KA, McQuiston AR, Guido W. Optogenetic stimulation of the corticothalamic pathway affects relay cells and GABAergic neurons differently in the mouse visual thalamus. PLoS One. 2012; 7:e45717. [PubMed: 23029198]

Katz LC. Local circuitry of identified projection neurons in cat visual cortex brain slices. J Neurosci. 1987; 7:1223–1249. [PubMed: 3553446]

Kim J, Matney CJ, Roth RH, Brown SP. Synaptic organization of the neuronal circuits of the claustrum. J Neurosci. 2016; 36(3):773–784. [PubMed: 26791208]

Kohlmeier KA, Ishibashi M, Wess J, Bickford ME, Leonard CS. Knockouts reveal overlapping functions of M(2) and M(4) muscarinic receptors and evidence for a local glutamatergic circuit within the laterodorsal tegmental nucleus. J Neurophysiol. 2012; 108:2751–2766. [PubMed: 22956788]

Kubasik-Juraniec J, Narkiewicz O, Morys J. Relationship of corticoclaustral axon terminals to neurons of the claustrum in the cat. Folia Morphol (Warsz). 1994; 53:69–76. [PubMed: 8001883]

LeVay S. Synaptic organization of claustral and geniculate afferents to the visual cortex of the cat. J Neurosci. 1986; 6:3564–3575. [PubMed: 2432202]

LeVay S, Sherk H. The visual claustrum of the cat. I. Structure and connections. J Neurosci. 1981; 1:956–980. [PubMed: 6169810]

Li J, Guido W, Bickford ME. Two distinct types of corticothalamic EPSPs and their contribution to short-term synaptic plasticity. J Neurophysiol. 2003; 90:3429–3440. [PubMed: 12890796]

Li J, Wang S, Bickford ME. Comparison of the ultrastructure of cortical and retinal terminals in the rat dorsal lateral geniculate and lateral posterior nuclei. J Comp Neurol. 2003; 460:394–409. [PubMed: 12692857]

Lyon DC, Jain N, Kaas JH. The visual pulvinar in tree shrews II. Projections of four nuclei to areas of visual cortex. J Comp Neurol. 2003; 467:607–627. [PubMed: 14624492]

Masterson SP, Li J, Bickford ME. Frequency-dependent release of substance P mediates heterosynaptic potentiation of glutamatergic synaptic responses in the rat visual thalamus. J Neurophysiol. 2010; 104:1758–1767. [PubMed: 20660425]

Montero VM. The interneuronal nature of GABAergic neurons in the lateral geniculate nucleus of the rhesus monkey: a combined HRP and GABA-immunocytochemical study. Exp brain Res. 1986; 64:615–622. [PubMed: 3026831]

Norita M, Hirata Y. Some electron microscope findings of the claustrum of the cat. Arch Histol Jpn. 1976; 39:33–49. [PubMed: 938201]

Ogren MP, Hendrickson AE. The morphology and distribution of striate cortex terminals in the inferior and lateral subdivisions of the Macaca monkey pulvinar. J Comp Neurol. 1979; 188:179–199. [PubMed: 115908]

Olson CR, Graybiel aM. An outlying visual area in the cerebral cortex of the cat. Prog Brain Res. 1983; 58:239–245. [PubMed: 6195690]

Olson CR, Graybiel AM. Sensory maps in the claustrum of the cat. Nature. 1980; 288:479–481. [PubMed: 7442793]

Piché M, Thomas S, Casanova C. Spatiotemporal profiles of receptive fields of neurons in the lateral posterior nucleus of the cat LP-pulvinar complex. J Neurophysiol. 2015; 114:2390–2403. [PubMed: 26289469]

Raczkowski D, Fitzpatrick D. Terminal arbors of individual, physiologically identified geniculocortical axons in the tree shrew's striate cortex. J Comp Neurol. 1990; 302:500–514. [PubMed: 1702114]

Rahman FE, Baizer JS. Neurochemically defined cell types in the claustrum of the cat. Brain Res. 2007; 1159:94–111. [PubMed: 17582386]

Remedios R, Logothetis NK, Kayser C. Unimodal responses prevail within the multisensory claustrum. J Neurosci. 2010; 30:12902–12907. [PubMed: 20881109]

Remedios R, Logothetis NK, Kayser C. A role of the claustrum in auditory scene analysis by reflecting sensory change. Front Syst Neurosci. 2014; 8:44. [PubMed: 24772069]

Reynhout K, Baizer JS. Immunoreactivity for calcium-binding proteins in the claustrum of the monkey. Anat Embryol (Berl). 1999; 199:75–83. [PubMed: 9924937]

Rockland KS, Andresen J, Cowie RJ, Robinson DL. Single axon analysis of pulvinocortical connections to several visual areas in the macaque. J Comp Neurol. 1999; 406:221–250. [PubMed: 10096608]

Sherk H, LeVay S. Visual claustrum: topography and receptive field properties in the cat. Science. 1981; 212:87–89. [PubMed: 7209525]

Sherman SM, Guillery RW. On the actions that one nerve cell can have on another: distinguishing “drivers” from “modulators”. Proc Natl Acad Sci U S A. 1998; 95:7121–7126. [PubMed: 9618549]

Smith JB, Radhakrishnan H, Alloway KD. Rat claustrum coordinates but does not integrate somatosensory and motor cortical information. J Neurosci. 2012; 32:8583–8588. [PubMed: 22723699]

Smythies J, Edelstein L, Ramachandran V. Hypotheses relating to the function of the claustrum. Front Integr Neurosci. 2012; 6:53. [PubMed: 22876222]

Smythies, J.Edelstein, L., Ramachandran, V., editors. The claustrum Structural, Functional and Clinical Neuroscience. Academic Press; 2014.

Usrey WM, Fitzpatrick D. Specificity in the axonal connections of layer VI neurons in tree shrew striate cortex: evidence for distinct granular and supragranular systems. J Neurosci. 1996; 16:1203–1218. [PubMed: 8558249]

Usrey WM, Muly EC, Fitzpatrick D. Lateral geniculate projections to the superficial layers of visual cortex in the tree shrew. J Comp Neurol. 1992; 319:159–171. [PubMed: 1375607]

Vidnyánszky Z, Borostyánkõi Z, Görcs TJ, Hámori J. Light and electron microscopic analysis of synaptic input from cortical area 17 to the lateral posterior nucleus in cats. Exp brain Res. 1996; 109:63–70. [PubMed: 8740209]

Vidnyánszky Z, Hámori J. Quantitative electron microscopic analysis of synaptic input from cortical areas 17 and 18 to the dorsal lateral geniculate nucleus in cats. J Comp Neurol. 1994; 349:259–268. [PubMed: 7860782]

Wasilewska B, Najdzion J. Types of neurons of the claustrum in the rabbit--Nissl, Klüver-Barrera and Golgi studies. Folia Morphol (Warsz). 2001; 60:41–45. [PubMed: 11234697]

Wilson CJ. GABAergic inhibition in the neostriatum. Prog Brain Res. 2007; 160:91–110. [PubMed: 17499110]

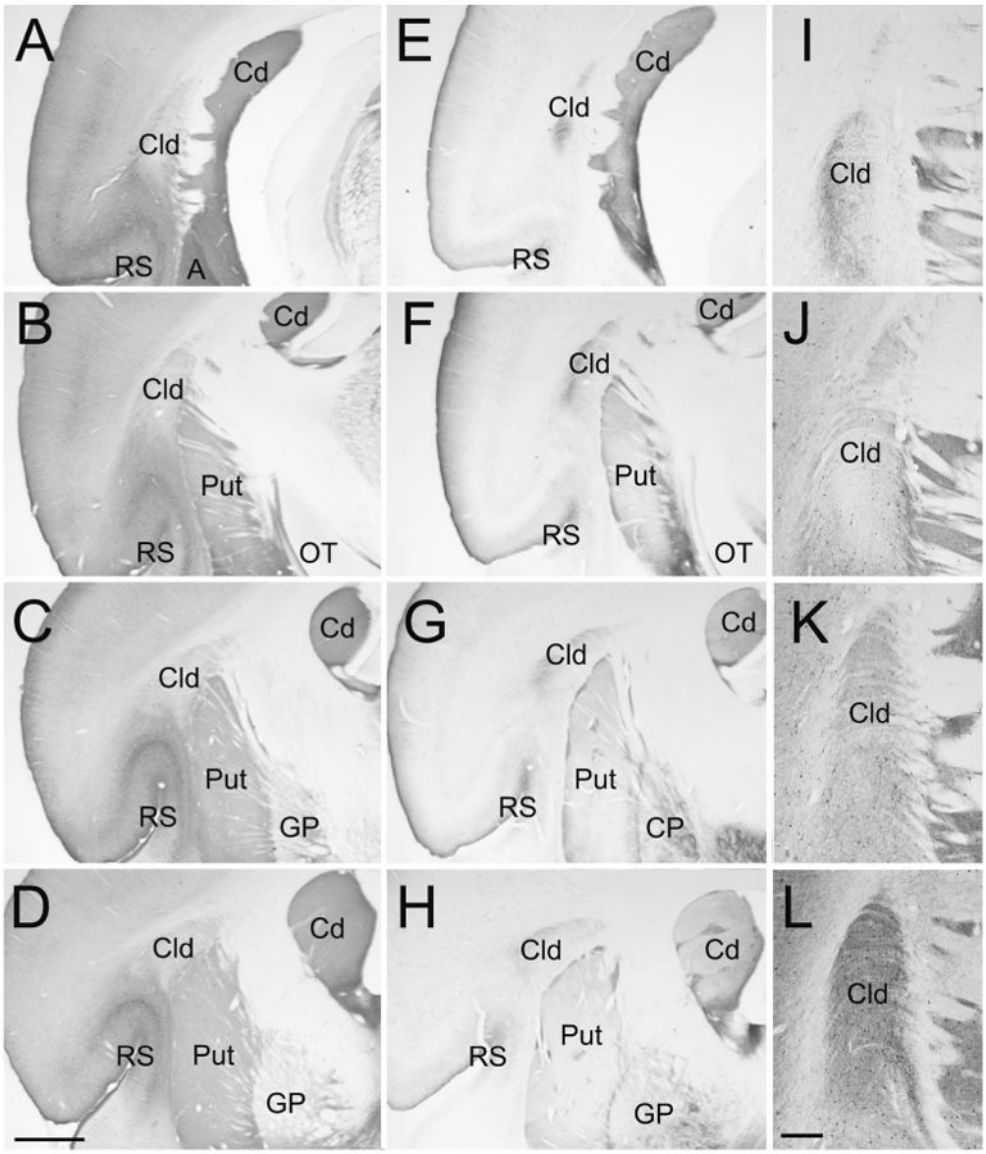

Figure 1. Cytoarchitecture of the tree shrew dorsal claustrum (Cld)

Sections stained with antibodies against calretinin (A-D, and J), substance P (E-H, and I), neuronal nitric oxide synthase (K), and parvalbumin (L) illustrate the location and staining characteristics of the Cld. Sections are all from the same animal. Sections A-D and E-H are arranged from caudal (A, E) to rostral (D, H) at intervals of 600 μm. Sections I-L are adjacent sections through the Cld arranged caudal (I) to rostral (L). A, amygdala, Cd, caudate nucleus, GP, globus pallidus, OT, optic tract, Put, putamen, RS, rhinal sulcus. Scale in D = 1 mm and applies to A-H. Scale in L = 250 μm and applies to I-L.

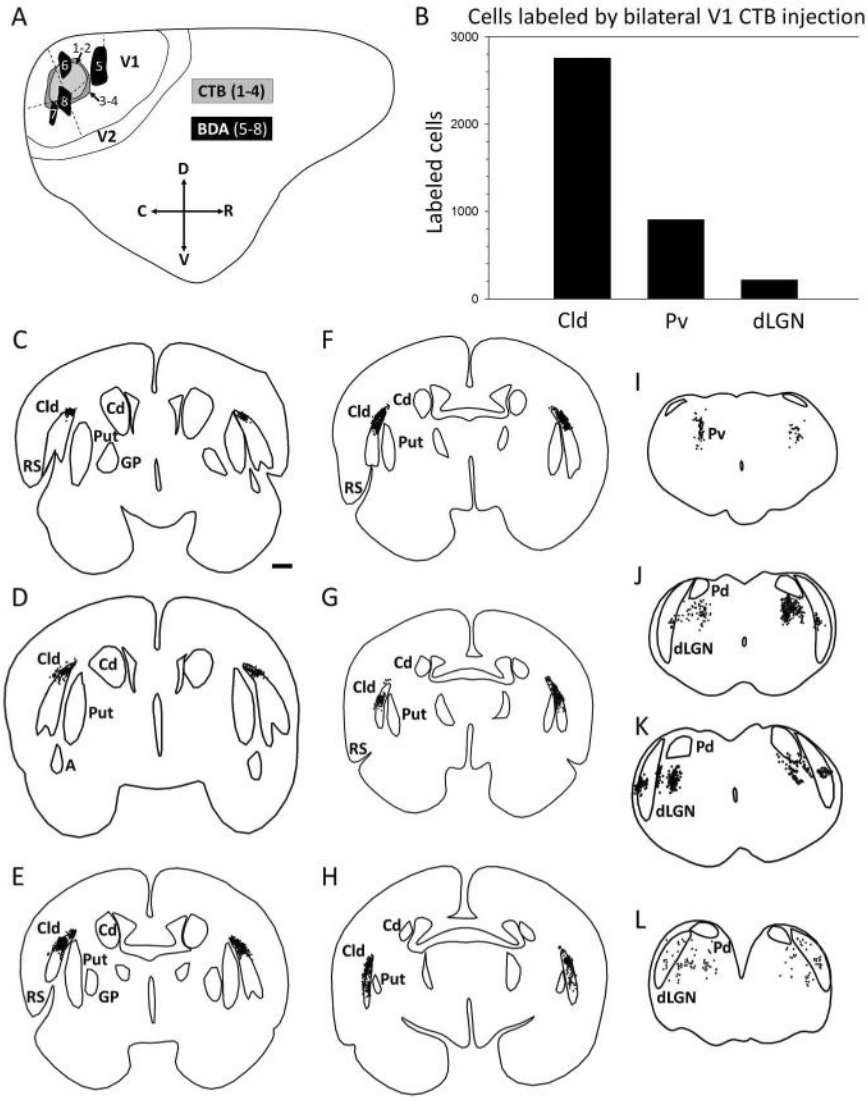

Figure 2. Distribution of claustrum and thalamus cells that project to V1

A) Diagrammatic representation of one cerebral hemisphere illustrates the placement of neuroanatomical tracer injections in V1. Locations of injections of the beta subunit of cholera toxin (CTB, labeled 1 – 4) were made to examine the distribution of cells projecting to V1 from dorsal claustrum (Cld), ventral pulvinar (Pv) and dorsal lateral geniculate nucleus (dLGN). Injections of biotinylated dextran amine (BDA, labeled 5 – 8) were placed in V1 to reveal the projections of V1 to Cld, Pv and dLGN. B) Histogram plotting the number of cells labeled in Cld. Pv and dLGN following bilateral CTB injection. C-L) Coronal sections (arranged rostral to caudal) show plots of cells labeled in one case as a result of bilateral CTB injections in V1. Black dots represent labeled cells. (Scale bar in C = 1 mm and applies to C – L. C, caudal; Cd; caudate; D, dorsal; GP, globus pallidus; Put, putamen, R, rostral; RS, rhinal sulcus; V, ventral.

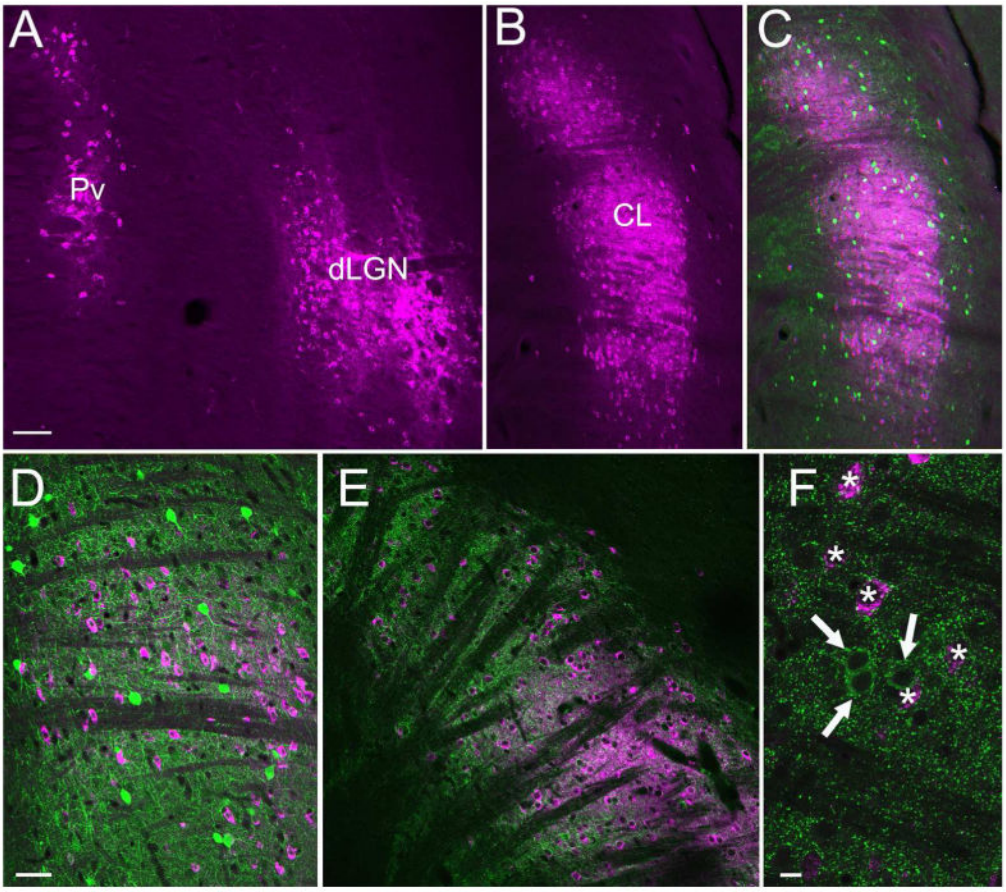

Figure 3. Claustrum cells that project to V1 are nonGABAergic and do not contain parvalbumin

Cells (purple) labeled by CTB injections in V1 are illustrated in confocal images (50 μm stacks) of the thalamus (A) and claustrum (B). Sections containing CTB-labeled claustrum cells were stained with antibodies against parvalbumin (green, C, 50 μm confocal stack and D, single 2 um optical section) or GAD (green, E, 25 μm confocal stack and F, single 1 μm optical section). No CTB-labeled claustrum cells were stained with antibodies against parvalbumin or GAD. Scale in A = 100 μm and also applies B and C. Scale in D = 50 μm and also applies to E. Scale in F = 10 μm.

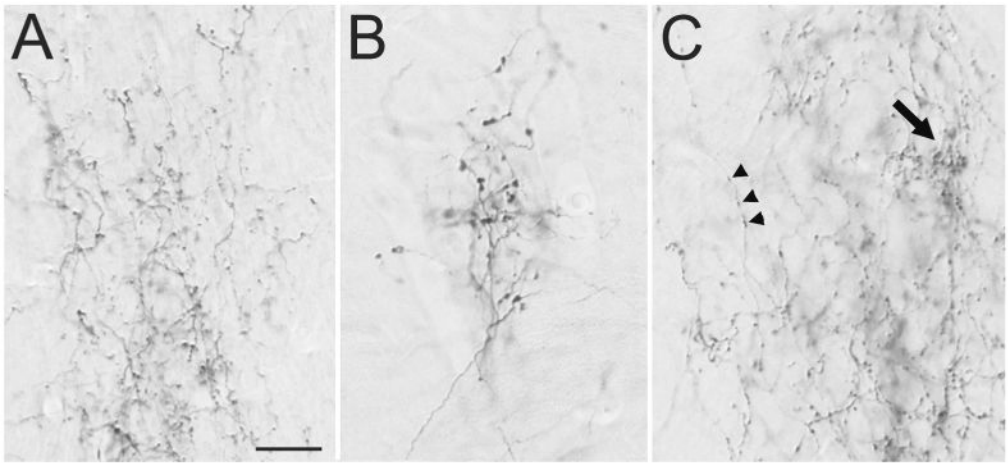

Figure 4. Morphology of V1 projections to the thalamus and claustrum

Light micrographs illustrate the morphology of axons labeled by an injection of biotinylated dextran amine in V1. A) V1 axons in the dorsal lateral geniculate nucleus form small boutons. B) V1 axons in the ventral pulvinar nucleus form clusters of large boutons. C) V1 axons in the dorsal claustrum form small boutons along thin axons (arrowheads), or dense clusters of slightly larger boutons (arrow). Scale = 20 μm and applies to all panels.

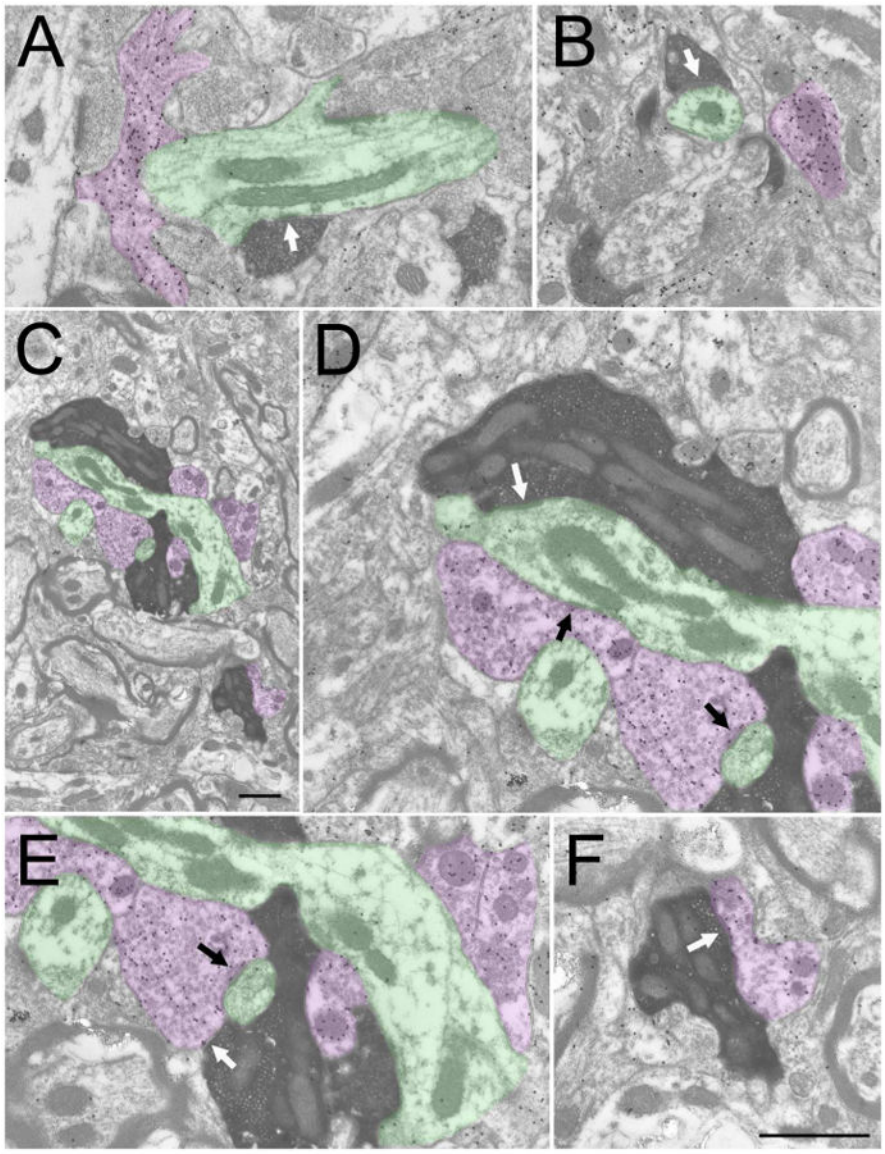

Figure 5. Ultrastructure of V1 projections to the thalamus

Electron micrographs illustrate the ultrastructure of corticothalamic terminals (dark reaction product) labeled by an injection of biotinylated dextran amine in V1. The tissue was additionally stained to reveal GABAergic (high density of gold particles, purple) and nonGABAergic (low density of gold particles, green) profiles. V1 terminals in the dorsal lateral geniculate nucleus (A and B) form small boutons that primarily contact (white arrows) small nonGABAergic dendrites. V1 terminals in the ventral pulvinar (Pv) nucleus (C) form large boutons that contact GABAergic and nonGABAergic dendrites in complex arrangements. A large V1-Pv terminal and associated GABAergic and nonGABAergic profiles is illustrated in (C, scale = 1 μm). The synaptic contacts (white arrows) of this terminal are illustrated at higher magnification in D (nonGABAergic dendrite), E and F (GABAergic dendritic terminals, F2 profiles). Synapses formed by associated GABAergic profiles are indicated by black arrows (D and E). Scale in F = 1 μm and applies to A, B, D-F.

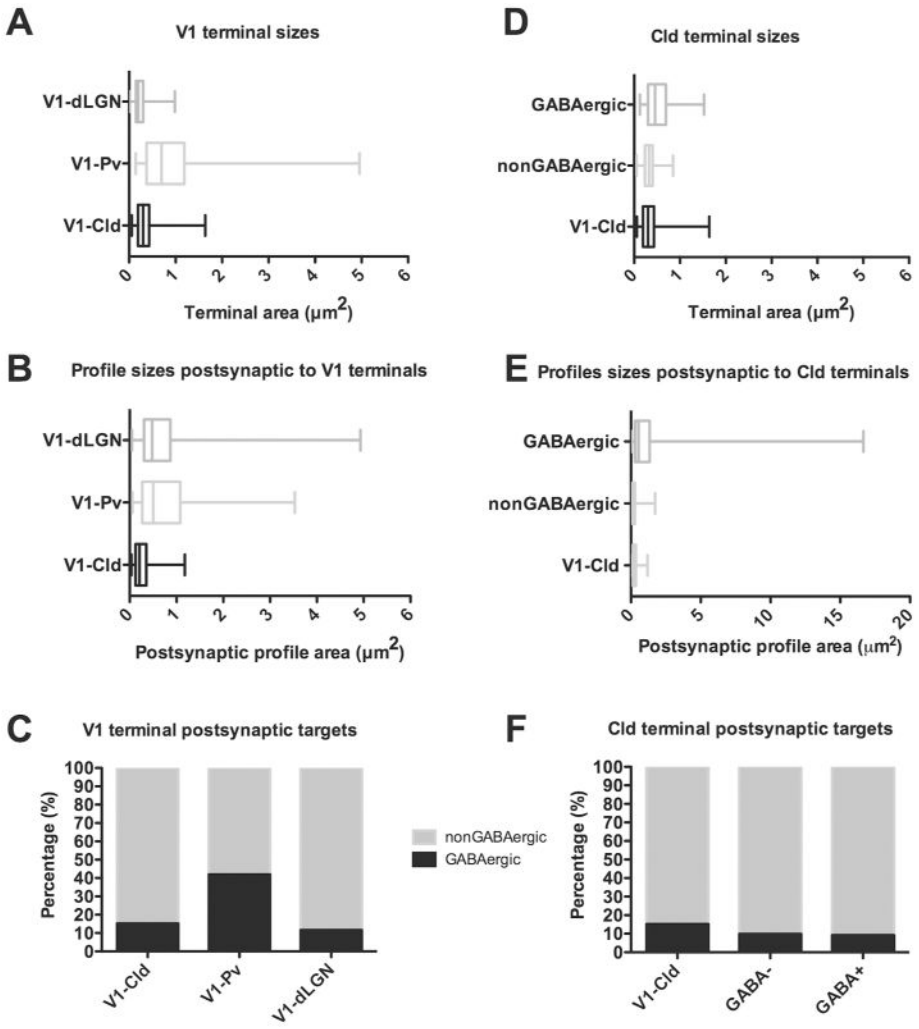

Figure 6. Quantification of circuits in the dLGN, Pv and Cld

A) Box and whisker plots illustrate the sizes of terminals in the dLGN (n=207), Pv (n= 101) and Cld (n=189) that originate from V1. The vertical bar within each box indicates the mean terminal size, the box boundaries indicate the lower and upper quartiles (25% and 75%), and the horizontal lines ("whiskers") indicate the full range of terminal sizes. The sizes of V1-dLGN, V1-Pv and V1-Cld terminals were significantly different from one another (Mann Whitney, $p < 0.0001$). B) Box and whisker plots illustrate the size of profiles postsynaptic to dLGN (n=207), Pv (n=131) and Cld (n=191) terminals that originate from V1. There was no significant difference between the size of dendrites postsynaptic to V1-dLGN and V1-Pv terminals ($p = 0.7296$), but dendrites postsynaptic to V1-Cld terminals were significantly smaller than dendrites postsynaptic to either V1-dLGN or V1-Pv terminals ($p < 0.0001$). C) Stacked histograms illustrate the percentage of GABAergic (black) and nonGABaergic (gray) profiles postsynaptic to V1-dLGN, V1-Pv and V1-Cld terminals. D) Box and whisker plots illustrate the sizes of V1-Cld terminals (n=189), the overall population of nonGABAergic terminals (n=244), and the overall population of GABAergic terminals (n=119) in the Cld. There was no significant difference between the size V1-Cld terminals and nonGABAergic terminals ($p= 0.2111$), but GABAergic terminals were significantly

larger than both V1-Cld terminals and nonGABAergic terminals ($p < 0.0001$). E) Box and whisker plots illustrate the size of profiles postsynaptic V1-Cld terminals (n=191), the overall population of nonGABAergic terminals (n=244), and the overall population of GABAergic terminals (n=119) in the Cld. Profiles postsynaptic to V1-Cld terminals were significantly larger than profiles postsynaptic to nonGABAergic terminals ($n = 0.0174$), and dendrites postsynaptic to GABAergic terminals were significantly larger than dendrites postsynaptic to either V1-Cld or nonGABAergic terminals ($p < 0.0001$). F) Stacked histograms illustrate the percentage of GABAergic (black) and nonGABaergic (gray) profiles postsynaptic to V1-Cld, nonGABAergic (GABA-), and GABAergic (GABA+) terminals in the Cld.

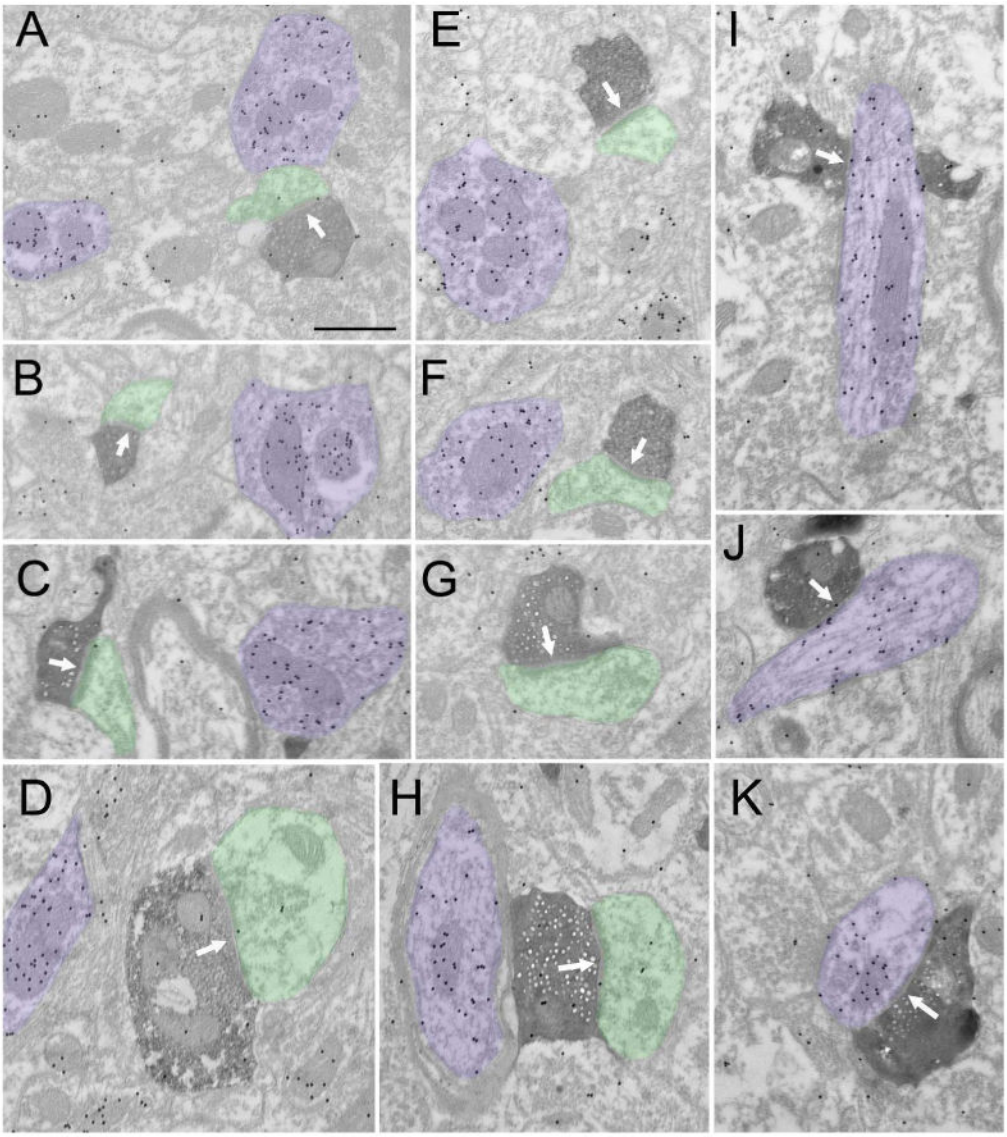

Figure 7. Ultrastructure of V1 projections to the claustrum

Electron micrographs illustrate the ultrastructure of corticoclaustral terminals (dark reaction product) labeled by an injection of biotinylated dextran amine in V1. The tissue was additionally stained to reveal GABAergic (high density of gold particles, purple) and nonGABAergic (low density of gold particles, green) profiles. Corticoclaustral primarily contact (white arrows) small nonGABAergic dendrites (A-H), but a small percentage (15%) contact GABAergic dendrites (I-K). Scale = 0.5 μm and applies to all panels.

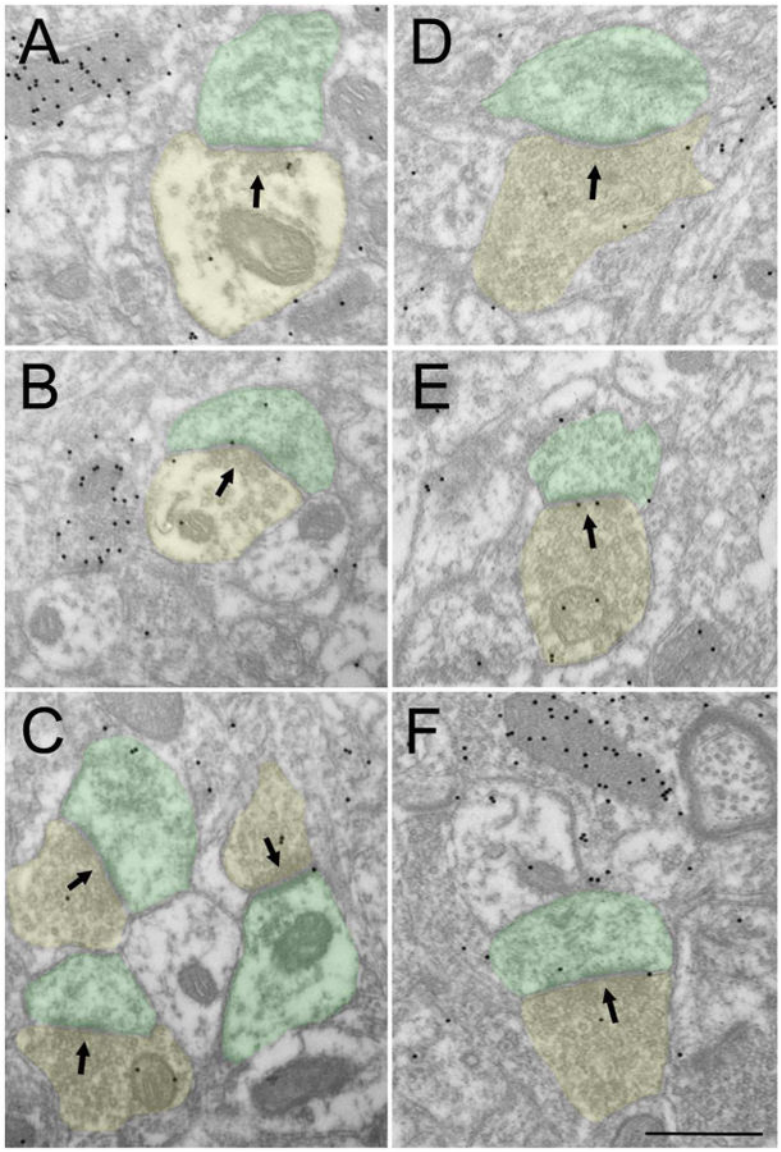

Figure 8. nonGABAergic terminal types in the claustrum

Electron micrographs illustrate the ultrastructure of nonGABAergic terminals (low density of gold particles, yellow) in the claustrum. NonGABAergic terminals contain sparse (A, B) or dense (C-F) vesicles and primarily contact (black arrows) small nonGABAergic dendrites (green). Scale = 0.5 μm and applies to all panels.

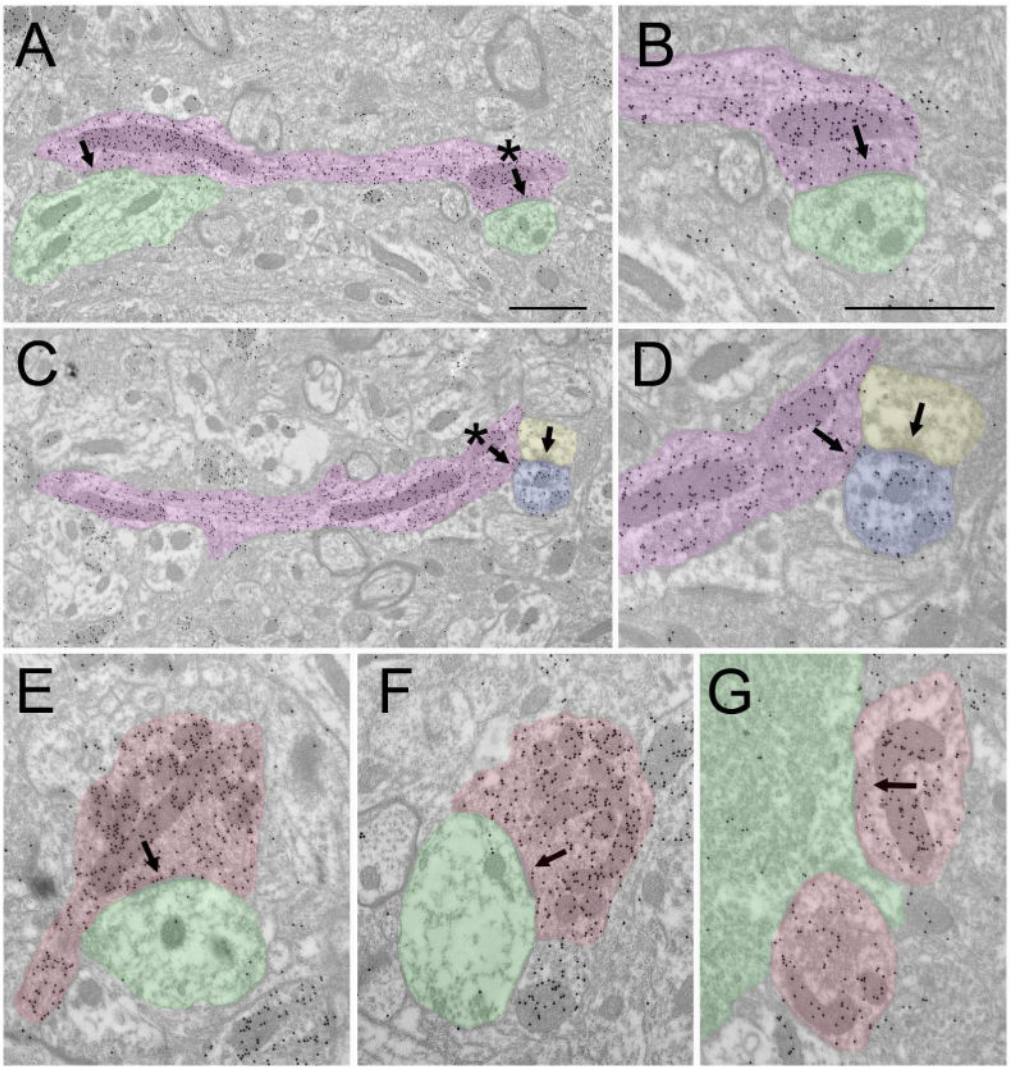

Figure 9. GABAergic terminal types in the claustrum

Electron micrographs illustrate the ultrastructure of GABAergic terminals (high density of gold particles) in the claustrum. GABAergic terminals that originate from dendrites (A-D, purple) contain vesicles that are clustered near synapses (arrows, asterisks in A and C indicate synapses shown at higher magnification in C and D). GABAergic dendritic terminals contact nonGABAergic dendrites (A, B, green) or GABAergic dendrites (B, D, blue; this dendrite also receives input from a nonGABAergic terminal, yellow). GABAergic terminals that presumably arise from axons (E-G, red) primarily contact nonGABAergic dendrites (E-F, green) and somata (G, green). Scale bar = 1 μm. Scale in A also applies to C. Scale in B also applies to D-G.

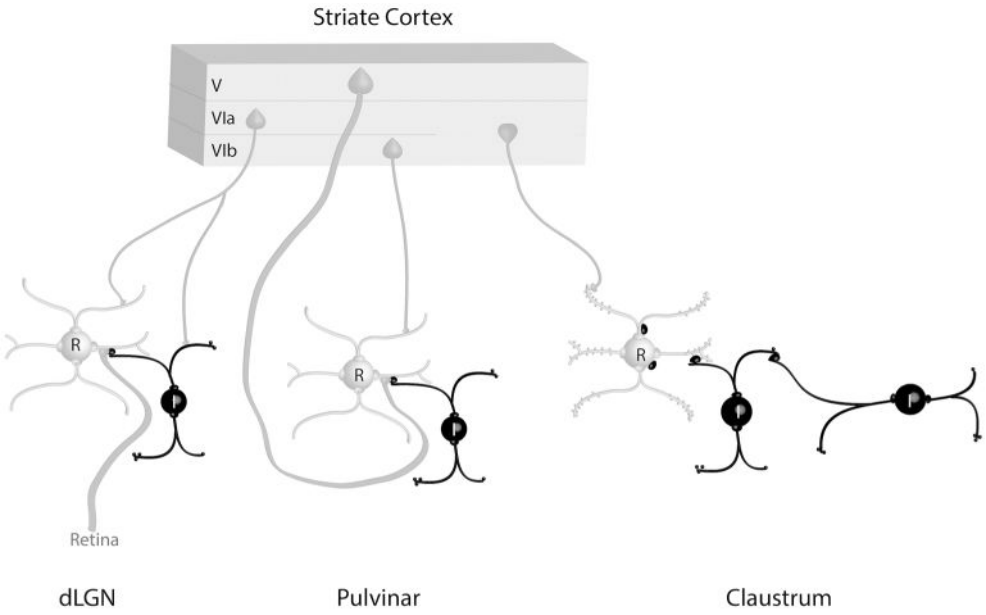

Figure 10. Schematic summary of circuits in the visual thalamus and claustrum

The schematic summary illustrates the contribution of terminals that originate from the tree shrew striate cortex to synaptic circuits in the dorsal lateral geniculate (dLGN), pulvinar nucleus, and claustrum. Interneurons (I) and other elements that contain gamma amino butyric acid (GABA) are black. Thalamocortical and claustrocortical cells (relay cells, R), and other elements that are nonGABAergic, are gray. Circuits identified in the claustrum suggest an integration of convergent cortical inputs, gated by GABAergic circuits. See text for details.

Table 1

Primary antibodies used in this study

Antigen	Description of immunogen	Source, host species, RRID	Concentration used
calretinin	Recombinant rat calretinin	Chemicon (Millipore), mouse monoclonal, MAB1568, RRID:AB_94259	1:5000 0.2 μg/ml
CTB	Toxin from Vibrio cholerae	Sigma-Aldrich, rabbit polyclonal, C3062, RRID:AB_258833	1:10,000 6.5 μg/ml
GABA	GABA conjugated to bovine serum albumin using glutaraldehyde	Sigma-Aldrich, rabbit polyclonal, A2052, RRID:AB_477652	1:2000 0.25 μg/ml
GAD67	Amino acid residues 4-101 of human GAD67	Chemicon (Millipore), mouse monoclonal, MAB5406, RRID:AB_2278725	1:1000 1 μg/ml
Neuronal nitric oxide synthase	C-terminal synthetic peptide sequence corresponding to amino acids (1419-1433) of human nNos coupled to keyhole limpet hemocyanin	Diasorin, rabbit polyclonal, 24287, RRID:AB_572256	1:8000 Concentration not applicable to whole serum
parvalbumin	Parvalbumin purified from frog muscle	Sigma-Aldrich, mouse monoclonal, P3088, RRID:AB_477329	1:5000 5.4 μg/ml
Substance P	Substance P conjugated to bovine serum albumin with carbodiimide.	Accurate Chemical Company, rat monoclonal (clone NC1/34), YMC1021, RRID:AB_2333091	1:500 Concentration not applicable to tissue culture supernatant